자성 나노 입자의 조절을 통한 MR 이미징에서의 T2 이완도 증강

노영준[1], 박요셉[1], 강병훈[1], 이재민[1], 허용민[2], 함승주[1†]

[1]120-749 서울특별시 서대문구 신촌동 연세대학교 화공생명공학과
[2]120-752 서울특별시 서대문구 신촌동 연세대학교 의과대학 영상의학과

Amplification of T2 relaxation rate in MR imaging via tuning magnetic seed nanoparticles

Youngjun Ro[1], Joseph Park[1], Byunghoon Kang[1], Jaemin Lee[1], Young-Min Huh[2] and Seungjoo Haam[1†]

[†1]Department of Chemical and Biomolecular Engineering, Yonsei University
Seoul 120-749, Republic of Korea
[2]Department of Radiology, College of Medicine, Yonsei University
Seoul 120-752, Republic of Korea

Keywords: Iron oxide nanoparticles, nanoclusters, T2 relaxivity

Abstract We describe the preparation of superparamagnetic nanoclusters (SNCs) by fine-tuning of the seed Fe_3O_4 nanoparticle sizes to enhance and their T2 relaxivity can be increased by > 4-fold. Therefore, with 11 nm seed core and PVA coating, SNC-11 exhibit a higher T2 relaxivity than other cluster condition. So fabricating the cluster, seed size is the most important influence the T2 relaxivity. As well as, in vitro cellular imaging results demonstrated the strong potential of SNCs for clinical applications by targeting affinity. According to the experiments, with 11 nm seed core and PVA coating, SNC-11 exhibited the highest T2 relaxivity of 454 $mM^{-1}s^{-1}$ due to the strong seed size effect on their magnetic sensitivity, indicating superior magnetic resonance (MR) contrast efficiency. Further in vitro cellular imaging results demonstrated the strong potential of SNCs for clinical applications.

1. Introduction

Organization of individual nanoparticles (NPs) into 2-D or 3-D nanostructures – superlattices or small clusters – motivated an opportunity to manufacture materials with enhanced physical, chemical and mechanical properties.[1-6] While individual NPs alone offer many scientific challenges and applications, ensembles of NPs show unique coupled properties that potentially can be applied in functional nanoscale materials which are important in biological diagnosis, catalysis, plasmonics, and data storage application.[3-5,7]

† E-mail : haam@yonsei.ac.kr

Currently, a number of theoretical and experimental studies have been conducted to examine the effectiveness of iron oxide nanoparticles in MR imaging. The transverse relaxation rate (r2) of water protons has demonstrated that the magnetization and size of the magnetic nanoparticles (MNPs) are key factors influencing the relaxation rate.[8,9] More specifically, studies have demonstrated an increase in relaxation rates with increasing magnetization. Accordingly, nanoparticles made from various compositions possessing high magnetizations have been synthesized, such as Mn- or Zn-doped ferrites, and resulted in a significant increase of the relaxation rate.[10,11] Although r2 can be enhanced by increasing the size of individual particles, this approach could be more difficult to assess due to the difficulties in achieving accurate sizes and size distributions. However, aggregates of MNPs have been shown to exhibit dramatically higher relaxation rates compared to single MNPs.[9,10] Clustering of individual MNPs is appealing as it provides a facile way to increase the overall magnetic content per particle, while still maintaining high colloidal stability. Strategies for preparing MNP-based contrast agents by controlled aggregation have yielded suitable colloidal materials for highly effective T2 contrast agents.[12-14]

Herein, we report on an optimal design strategy of superparamagnetic nanoclusters (SNCs), capable of achieving a high r2 relaxivity through the control of the seed nanoparticles (Figure. 1). The size of the seed nanoparticles has been controlled from 4 to 11 nm encapsulated within a polyvinyl alcohol (PVA, Mw 13,000 ~ 23,000 g/mole) shell to form superparamagnetic nanoclusters (SNCs), and they showed excellent colloidal stability under various physiological conditions. The saturation magnetization of SNCs increased with increasing seed nanoparticles. The resultant SNCs possess a large magnetic content and produce a strong magnetic field exhibiting a high r2 relaxivity (454 $mM^{-1}s^{-1}$[metal])due to magnetic coupling effect.[11,12] Subsequent application of SNCs to a cellular assay system was performed to assess their use in identifying biomarkers and target cells.[15]

Dual imaging capacity was further demonstrated using magnetic resonance (MR) and fluorescence imaging.[16]

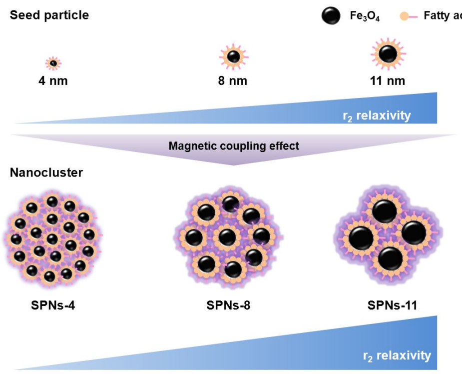

Figure 1. Schematic illustration of high performance superparamagnetic nanoclusters (SNCs) for use as a T2 contrast agent. The gradient blue color bar represents the transverse relaxivity (r2) strength corresponding to core sizes.

2. Materials and Methods

2.1. Materials

Iron(Ⅲ) acetylacetonate ($Fe(acac)_3$), 1,2-hexadecandiol, oleylamine, oleic acid, benzyl ether, phenyl ether, bromoacetic acid, pyrene, poly vinyl alcohol (PVA, Mw 13,000 ~ 23,000 g/mole), were purchased from Sigma-Aldrich (St. Louis, USA). Hexane and ethanol were obtained from Duksan pure chemicals Co. (Korea). Ultrapure deionized water was used for all of the synthesis. All other chemicals and regents were of analytical grade.

2.2. Synthesis of iron oxide magnetic nanoparticles

The synthesis of 4 nm nanoparticles is as follows[19]: Iron (Ⅲ) acetyl acetonate, 1, 2-hexadecandiol, oleic acid, oleyl amine, phenyl ether was mixed in a two neck flask, and then the mixture was placed in a 110 ℃ vacuum condition for 30 minutes to eliminate the moisture and oxygen. The mixture was heated to 200℃ for 30 minutes to form Fe_3O_4 seed particles. Next, the product was heated to 265 ℃ for 30 minutes to growth the particles.

The 8 nm particles were also synthesized by a similar method. Iron (Ⅲ) acetyl acetonate, 1, 2-hexadecandiol, oleic acid, and oleyl amine were also used, but to make the 8 nm particles, we changed the solvent to benzyl ether. Since benzyl ether has higher boiling temperature than phenyl ether, it is more suitable for high temperature reaction.

All ingredients were mixed in a two neck flask, which was placed in a 110 ℃ vacuum condition for 30 minutes to eliminate the moisture and oxygen. Subsequently, the mixture heated to 200℃ for two hours to form Fe_3O_4 seed particles. Next, the product was heated to 300℃ for one hour to grow the particles.

Eleven nanometer particle ingredients were same as the 8 nm particles except for adding 8 nm particles as a seed. The 8 nm particles were dispersed with 4 ml of hexane. To reduce overflow during the synthesis, the mixture was place in a room temperature vacuum condition for 30 min. and 110℃ vacuum condition for an excess of 30 minutes. The mixture was heated to 200℃ for one hour, then 300℃ for 30 minutes. The product of all magnetic nanoparticle synthesis reactions were washed with 20 ml ethyl alcohol.

Specifically, we added 20 ml ethyl alcohol to the end of synthesized product. The mixture was centrifuged at 6,000 rpm for 10 min. After centrifugation, the precipitated sample was present on the floor of centrifugation cell. The precipitant was dissolved with an appropriate hexane quantity, and the 20 ml of ethyl alcohol already present, centrifuged at 6,000 rpm for 10 min., and then the supernatant was discarded.

2.3. Fabrication and sorting of clusters

In this paper, we fabricate clusters using the emulsification method. First, PVA (200 mg) was dissolved in distilled water (20 ml) while shaking and heating the solution. MNP was dispersed with 4 ml of hexane. The PVA solution was then poured in the 100 ml beaker and the MNC dispersed solution was introduced by injection method under sonication condition. The mixture was stirred at 1,200 rpm for 15 min; subsequently we stored the mixture at room temperature overnight. Upon centrifuging the mixture solution, we obtained SNCs capping with PVA.

To fabricate a cluster using an emulsion process, it has the disadvantage of yielding a variety of cluster, so we performed sorting process to obtain similar sized clusters. The sample was centrifuged at different speeds since the heavy clusters required a low centrifugal force and light clusters required a high centrifugal force. Usually we repeated centrifugation at three different rpm (8,000, 10,000, 12,000 rpm) to perform separation by cluster size.

2.4. Synthesis of CMPVA

Synthesis of carboxymethyl polyvinyl alcohol (CMPVA): polyvinyl alcohol (6 g) was dissolved in distilled water (40 ml) using sonication and heating the solution. With vigorous stirring at room temperature sodium hydroxide solution (concentration: 5 g/ 10 mL) was added slowly into the PVA solution. After cooling the solution to room temperature, bromoacetic acid (10 g) in water (10 mL) was added drop-wisely into the mixture. [17]

The solution was stirred overnight at room temperature and neutralized with the addition of hydrochloric acid (1 M). Excess ethanol was added to precipitate the CMPVA, which was then collected by centrifugation for 10 min. at 4,000 rpm. CMPVA was purified by dispersing the polymer in 95% ethanol and removing the excess reactants. The purified polymer was freeze dried under vacuum at -30°C and stored at room temperature.

2.5. Antibody conjugation of SNC

To conjugate the antibody with the SNC, 0.1 mg of cetuximab was dissolved in 10 mM sodium phosphate buffered solution (400 μL, pH 7.4) and mixed with the above SNC solution (5 mg/mL).[18] Then, EDC (2.0 mmol) and NHS (2.0 mmol) were added to the solution. The amount of antibody conjugated with the SNCs was calculated using a BCA (bicinchoninic acid) kit. The irrelevant antibody (IRR, human IgG as a control)-conjugated SNC were synthesized in the manner described above.

2.6. Characterization

Morphology and size were analyzed by transmittance electron microscopy (TEM, JEM-2010, JEOL Ltd) and field emission scanning electron microscopy (SEM, S-900, Hitachi Ltd). Size distribution of MNCs was measured by laser scattering (DLS, ELS-Z, Otsuka electronics). Thermogravimetric analysis (TGA, SDT Q600, TA instruments Ltd.) was performed to determine the weight content of the particles and synthesized clusters. Fourier transform infrared spectroscopy (FT-IR, Excalibur series, Varian Inc.) analysis was performed to confirm the characteristic bands of the synthesized clusters. The saturation of magnetization was evaluated using a vibrating-sample magnetometer (VSM, Model 7400, Lakeshore). The amount of metals in the nanoparticles was determined by inductively coupled plasma optical emission spectroscopy (ICP-OES, INPREPID 2XSP, IRIS). To confirm the crystallinity, we used the X-ray diffraction (XRD, Ultima III, Rigaku). MR was performed at 1.5 T, and room temperature using a Micro-47 surface coil (MRI, Intera, Philips Medical Systems).

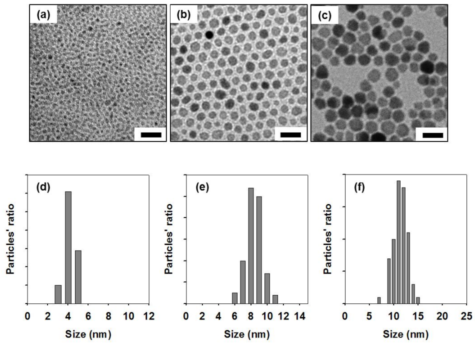

Figure 2. (a–c) TEM image of MNPs (superparamagnetic nanoparticles). (a):MNP–4, (b):MNP–8, (c):MNP–11 (scale bar = 20nm), and (d–f) Particles' size distribution by TEM image analysis. (d):MNP–4, (e):MNP–8, (f):MNP–11

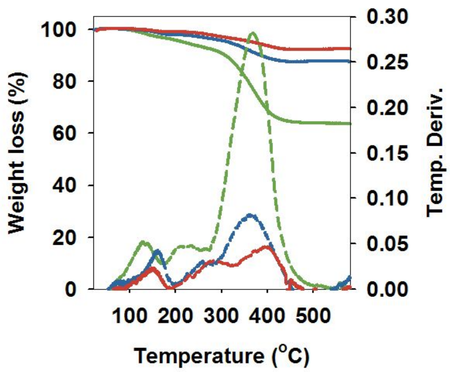

Figure 3. Thermogravimetric analysis (TGA) of magnetic nanoparticle (MNP). MNP–4 (green), MNP–8 (blue), and MNP–11 (Red). Dashed line means temperature derivate weight.

3. Result and Discussion

Thermal decomposition of the iron acetylacetonate complexes in the presence of hydrophobic surfactants and diol reducing agents resulted in the formation of spherical particles. By modifying the seed-mediated growth procedure as previously reported[19] to incrementally grow the magnetic core from 4 nm to 11 nm, we produced highly monodisperse MNPs soluble in organic solvent confirmed by TEM images of MNP-4 (3.7 ± 0.5 nm, size variation < 4.2 %), MNP-8 (7.9 ± 1 nm, size variation < 5 %) and MNP-11 (10.8 ± 1.5 nm, size variation < 3.1 %), respectively (Figure 2). Next, their ligand composition weight ratios measured by TGA revealed 36.2 % (MNP-4), 12.1 % (MNP-8) and 7.5 % (MNP-11), respectively (Figure 3).

This decrease of ligand ratio according to size increase of MNP is possibly due to their different surface area per volume. Precisely, the surface area per volume of MNP-4 was 1.5/ nm whereas the one of MNP-11 was 0.54/ nm.

Next we fabricated SNCs using seed nanoparticle sizes of 4 nm (SNC-4), 8 nm (SNC-8) and 11 nm (SNC-11). To evaluate the surfactant potential, the critical micelle concentration (CMC) of PVA was measured using fluorescence technique (Figure. 4). When the micelles were formed, the slope of fluorescence against the concentration of PVA decreased because the micelle was formed, pyrene entered micelle in the aqueous phase, and then pyrene emission intensity was changed. As the PVA concentration increased, the fluorescence intensity ratio of PVA (I_{390}/I_{375}) spontaneously declined with the critical micelle concentration of 82.2 nM. These results indicated that the PVA successfully played a role of surfactant for fabrication of clusters.

Upon evaporation of the low boiling point solvent (hexane), the nanoparticles confined

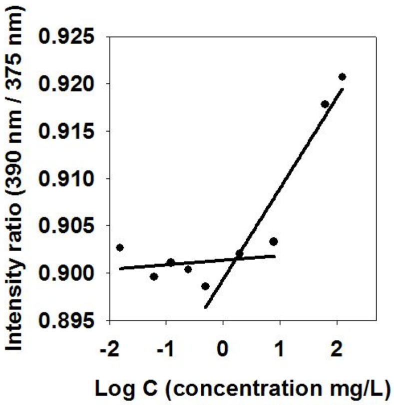

Figure 4. Plot of log C vs. intensity ratio (I_{390}/I_{375}) from the PVA solution emission spectrum. The critical micelle concentration is determined by taking the in flexion of the sigmoidal curve. The CMC of PVA is 1.48 mg/L(82.2nM).

the oil droplets were self-assembled into nanospheres, with the cluster size being controlled by adjusting the nanoparticle concentration or the extent of stirring speed during the emulsification process.[13] After solvent evaporation, nanometer-sized and monodisperse superparamagnetic clusters were finally formed. TEM images showed iron oxide magnetic nanoclusters using 4 nm, 8 nm, and 11 nm seed nanoparticles, with similar overall sizes of approximately 60 nm (57.3 ± 7.3 nm, Figure 5 a-c). In addition, FE-SEM indicated their fairly high monodispersities (Figure. 5 d-f). From the measurement of hydrodynamic diameters using dynamic light scattering (DLS), the mean sizes of SNC-4, SNC-8, and SNC-11 were similar at 73.3 nm, 78.1 nm, and 76.6 nm, respectively (Figure. 6a). PVA composition weight ratios of SNCs calculated from TGA analysis were 6.69 %

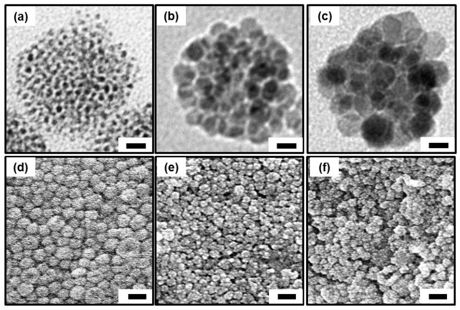

Figure 5. (a–c) TEM images of SNCs (Scale bar = 10 nm). (d–f) FE-SEM images of SNCs (Scale bar =50 nm). SNC-4 (a, d), SNC-8 (b, e), and SNC-11 (c, f)

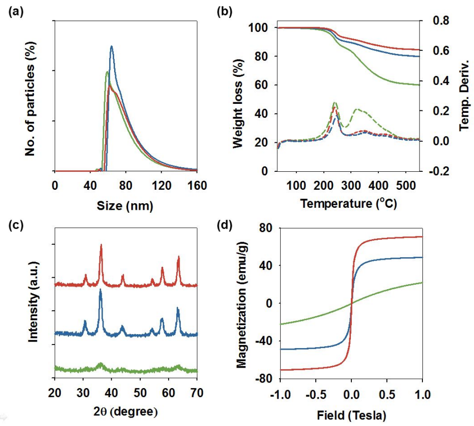

Figure 6. (a) Hydrodynamic size distributions with particle No.-weighted histograms, (b) thermo gravimetric weight losses to demonstrate of organic/inorganic compositions, (c) X-ray diffractometer analysis for spinel ferrite crystallinity, and (d) hysteresis loops for superparamagnetic behaviors at room temperature, SNC-4 (green line), SNC-8 (blue line), and SNC-11 (red line).

(SNC-4), 11.7 % (SNC-8) and 9.5 % (SNC-11), respectively, indicating that MNPs

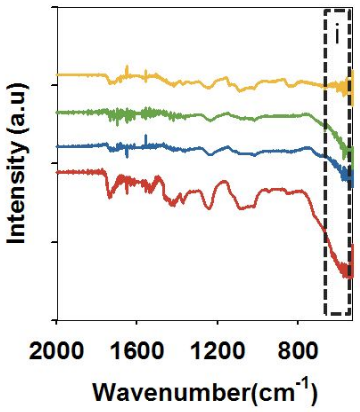

Figure 7. FT-IR of SNC-4 (red), SNC-8 (blue), SNC-11 (green), and PVA (yellow). Region (i) is the Fe-O bond peak.

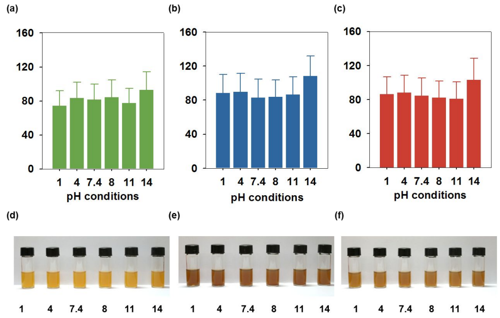

Figure 8. Colloidal pH stability tests. (a-c) Hydrodynamic diameter of SNCs in different pH condition (a): SNC-4, (b): SNC-8, (c): SNC-11. (d-f) Photographs of SNCs dispersed in different pH solutions (d: SNC-4, e: SNC-8, f: SNC-11).

were surrounded with a small amount of PVA molecules (Figure. 3, Figure. 6b).

The crystallinity of the as-prepared SNCs was analyzed by XRD (Figure. 6c) and all of the reflection peaks of SNCs indicated that the clusters were composed of iron oxide nanoparticles. In addition, we observed that larger the primary particles, more increase in the sharpness of peak. The Scherrer formula was used to estimate the average grain sizes of the clusters where D is the diameter of the grains, λ is the X-ray wavelength in nanometers (λ = 1.5418 Å), β is the width of the XRD peak at half-peak height in radians, and Θ is the angle between the incident and diffracted beams in degrees[20]. The grain sizes of seed Fe_3O_4 nanoparticles in SNC-4, SNC-8 and SNC-11 were confirmed as 4.3 nm, 8.3 nm and 11.8 nm, respectively.

FT-IR spectroscopy analysis performed on freeze dried samples of SNC-4, SNC-8 and SNC-11 (Figure. 7) showed that SNCs exhibited the characteristic bands of magnetite at 550 cm^{-1}(Fe-Ostretching).[3]

The magnetic properties analyzed using a VSM (Figure. 6d) showed that the magnetic hysteresis loops of SNC-4, SNC-8 and SNC-11 were observed at 300 K exhibiting superparamagnetic behavior without remanence coercivity at zero field. The saturation of magnetization values (Ms) of SNC-4, SNC-8, and SNC-11 were 24, 49 and 75 emu/g at 1 T, respectively.

In Figure. 8, colloidal stabilities of SNCs under various pH conditions were examined using dynamic light scattering (DLS), which showed that the hydrodynamic sizes (D_H) of SNC-4, SNC-8 and SNC-11 were highly stable over a wide pH range (3~11). The photographs of SNCs dispersed in different pH solutions also confirmed their remarkable broad tolerance at several pH levels. Therefore, PVA used as a surfactant in this

Table1. Comparison between the commercial contrast agent and our synthesized contrast agent.

Contrast agent	Seed particle		Surfactant	M_S^*	H_D^*	$r2^*$
	Materials	Size (nm)				
CLIO	Fe_3O_4	5	Dextran	45	30	62
Feridex	Fe_3O_4, γ-Fe_2O_3	4.96	Dextran	60	160	120
SNC-4	Fe_3O_4	60	PVA	24	73.3	111
SNC-8	Fe_3O_4	60	PVA	49	78.1	294
SNC11	Fe_3O_4	60	PVA	70	76.6	454

* M_S: Magnetic saturation value (emu /g), H_D: Hydrodynamic diameter(nm) of cluster , and r2: Transverse relaxation rate at 1.5T($mM^{-1}S^{-1}$)

one-pot reaction process[21] could sufficiently stabilize the nanoparticle clustering in a wide pH range due to hydrogen bonding between OH group and water, which could enable dispersion of SNCs in H_2O or phosphate buffered saline (PBS) without further surface modification.

In MR imaging, the contrast enhancement effects are directly related to the M_S value of the nanoparticles. Specifically, transverse relaxivity (R2=1/T2) represents the degree of T2-weighted MRI contrast effect where the R2 value is proportional to the M_S value. The size effects of iron oxide nanoparticles on the MRI contrast enhancements were measured at 1.5 T and compared with conventional iron oxide nanoparticles (Feridex, cross-linked iron oxide (CLIO) and Resovist) in table 1. The relaxivity coefficient (r2), which was obtained as the gradient of the plot of R2 versus the molarity of magnetic atoms, increased as the seed nanoparticle size increased by showing 110, 250 and 454 mM^{-1} s^{-1} for SNC-4, SNC-8 and SNC-11, respectively (Figure. 9). The r2 values of CLIO and Feridex were 62 mM^{-1} s^{-1} and 110 mM^{-1} s^{-1}, respectively (table 1). It is well accepted that, for assembled structures, magnetic dipole-dipole interactions are much stronger than those of individual nanoparticles, as a result of the anisotropy coupling effect of dipoles[12]. Therefore, interparticle magnetic coupling can increase overall individual magnetic anisotropy properties and raise the net positive magnetic force of clusters toward external magnetic field. In our work, neither a significant increase nor decrease of coercivity of SNCs as compared to individual NPs was observed as in most random nanoparticle aggregates as previously observed in Figure. 6d. Consequently, this increase in the relaxivity coefficient of SNCs is likely due to the presence of both anisotropic and random dipole-dipole interactions within the clusters, which makes SNCs behave superparmagnetically.

To investigate further capability of SNCs for cell labeling, we modified the repeating hydroxyl units of PVA into carboxylate

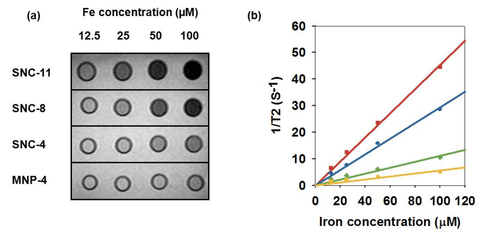

Figure 9. (a) T2-weighted MR image of aqueous solution of SNC-11, SNC-8, SNC-4, and MNP-4 (b) T2-weighted MR relaxation rate of SNC-11 (red), SNC-8 (blue), SNC-4 (green), and MNP-4 (yellow).

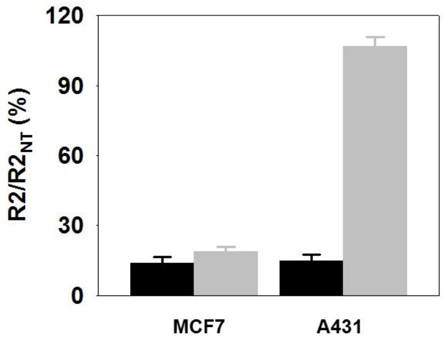

Figure 10. $\triangle R2/R2_{NT}$ graph against A431 and MCF7 cells incubated with CET - CMSNC-11(gray) and IRR - CMSNC-11 (black).

groups to form carboxymethyl PVA (CMPVA)[17]. Carboxymethylation is a common procedure in polysaccharide chemistry for derivatizing alcohol groups with carboxymethyl groups. The SNC-11 encapsulated with CMPVA (CMSNC-11) was prepared with a similar procedure as previously described. A431 cells, which have a high level of the EGFR cancer markers, were compared with MCF7 cells, which have a low level of the EGFR cancer markers. To compare the performance of CMSNC-11 in these cell lines, CMSNC-11 nanoparticles were conjugated with an anti-EGFR antibody (CET, cetuximab) utilizing the carboxyl group on the surface of the CMSNC-11. The targeting efficacy of Cetuximab conjugated CMSNC-11 (CET-CMSNC-11) and their detection by MR imaging were investigated using cancer cell lines. The cells were incubated with CET-CMSNC-11 at room temperature with a relatively short incubation time (2 h) to minimize the particle uptake via endocytosis.

The difference of $\triangle R2/R2_{NT}$ (NT;non-treated,$R2=T2^{-1}$) in the cells treated with CET-conjugated CMSNC-11 (CET-CMSNC-11) compared to those of CMSNC-11 conjugated with an irrelevant antibody (IRR, humanIgG;IRR-CMSNC-11) were approximately 119%(A431) and 22%(MCF7), respectively (Figure. 10). In addition, CET-CMSNC-11 exhibited specific affinity (5.4times) for A431 cells compared with MCF7 cells, demonstrating the efficient targeted delivery of CET-CMSNC-11 forth eEGFR receptor. IRR-CMSNC-11 treated cells, however, showed partial enhancement against the MR signal intensity owing to non-specific binding. Inaddition, the confocal microscopic images showed that A431 cells incubated with CET-CMSNC-11 presented excellent uptake efficiency compared to other cases (Figure. 11). In the case of A431 cells treated with CET-CMSNC-11, a bright red color was observed in the microscopic image,whereas dim fluorescence was noted for the IRR-CMSNC-11. Microscopic results demonstrated that

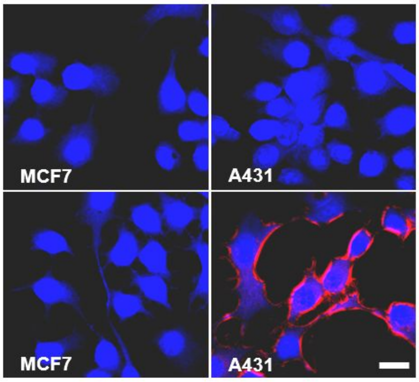

Figure 11. Confocal microscopy images of A431 and MCF7 cells incubated with CET - CMSNC-11 and IRR - CMSNC-11 at room temperature for 2h.

CET-CMSNC-11 successfully binds to A431 cells. Therefore, by using the well-defined SNCs as bimodal probes, we could specifically detect EGFR-expressing cancer cells using both fluorescence microscopy and MRI.

5. Conclusions

In summary, we suggest a strategy for preparing highly potent and functional superparamagnetic nanoclusters (SNCs). For a given magnetic material, SNCs are able to achieve high r2 relaxivity with densely packed magnetic nanoparticles. This is possibly due to the increase of magnetic anisotropic property by the magnetic coupling effect, as well as the net positive magnetic force, which together lead the SNCs to be highly effective MR contrast agents. The PVA shell in particular renders the particles highly soluble in aqueous media and can be utilized for surface conjugation. In addition, CMPVA by further modification of PVA provides a versatile bioconjugation moiety to serve as smart and bimodal contrast agents. We envisage that our SNCs could be readily extended to other magnetic nanocluster formations (e.g., Fe, CoFe, and MnFe), which could further improve the r2 relaxivity along with multimodal imaging and/or therapeutic treatment agents.

Acknowledgement

This study was supported by a grant of the Korea Health 21 R&D Project, Ministry of Health &Welfare, Republic of Korea. (A085136)

참고문헌

[1] G.H. Lee, S.H. Huh, J.W. Jeong, B.J. Choi, S.H. Kim, H.-C. Ri, Anomalous Magnetic Properties of MnO Nanoclusters, Journal of the American Chemical Society, 12094-12095, 124 (2002).

[2] J. Xie, X. Bu, N. Zheng, P. Feng, One-dimensional coordination polymers containing penta-supertetrahedral sulfide clusters linked by dipyridyl ligands, Chemical Communications, 4916-4918, (2005).

[3] S.-B. Seo, J. Yang, T.-I. Lee, C.-H. Chung, Y.J. Song, J.-S. Suh, H.-G. Yoon, Y.-M. Huh, S. Haam, Enhancement of magnetic resonance contrast effect using ionic magnetic

clusters, Journal of Colloid and Interface Science, 429-434, 319 (2008).

[4] J.-F. Berret, N. Schonbeck, F. Gazeau, D. El Kharrat, O. Sandre, A. Vacher, M. Airiau, Controlled Clustering of Superparamagnetic Nanoparticles Using Block Copolymers: Design of New Contrast Agents for Magnetic Resonance Imaging, Journal of the American Chemical Society, 1755-1761, 128 (2006).

[5] S. Singamaneni, V.N. Bliznyuk, C. Binek, E.Y. Tsymbal, Magnetic nanoparticles: recent advances in synthesis, self-assembly and applications, Journal of Materials Chemistry, 16819-16845, 21 (2011).

[6] J. Ge, Y. Hu, M. Biasini, W.P. Beyermann, Y. Yin, Superparamagnetic Magnetite Colloidal Nanocrystal Clusters, Angewandte Chemie International Edition, 4342-4345, 46 (2007).

[7] N. Koukabi, E. Kolvari, A. Khazaei, M.A. Zolfigol, B. Shirmardi-Shaghasemi, H.R. Khavasi, Hantzsch reaction on free nano-Fe2O3 catalyst: excellent reactivity combined with facile catalyst recovery and recyclability, Chemical Communications, 9230-9232, 47 (2011).

[8] J. Park, E. Lee, N.-M. Hwang, M. Kang, S.C. Kim, Y. Hwang, J.-G. Park, H.-J. Noh, J.-Y. Kim, J.-H. Park, T. Hyeon, One-Nanometer-Scale Size-Controlled Synthesis of Monodisperse Magnetic Iron Oxide Nanoparticles, Angewandte Chemie, 2932-2937, 117 (2005).

[9] Y.-w. Jun, Y.-M. Huh, J.-s. Choi, J.-H. Lee, H.-T. Song, KimKim, S. Yoon, K.-S. Kim, J.-S. Shin, J.-S. Suh, J. Cheon, Nanoscale Size Effect of Magnetic Nanocrystals and Their Utilization for Cancer Diagnosis via Magnetic Resonance Imaging, Journal of the American Chemical Society, 5732-5733, 127 (2005).

[10] Y.-w. Jun, J.-H. Lee, J. Cheon, Chemical Design of Nanoparticle Probes for High-Performance Magnetic Resonance Imaging, Angewandte Chemie International Edition, 5122-5135, 47 (2008) .

[11] J.-H. Lee, Y.-M. Huh, Y.-w. Jun, J.-w. Seo, J.-t. Jang, H.-T. Song, S. Kim, E.-J. Cho, H.-G. Yoon, J.-S. Suh, J. Cheon, Artificially engineered magnetic nanoparticles for ultra-sensitive molecular imaging, Nat Med, 95-99, 13 (2007).

[12] P. Qiu, C. Jensen, N. Charity, R. Towner, C. Mao, Oil Phase Evaporation-Induced Self-Assembly of Hydrophobic Nanoparticles into Spherical Clusters with Controlled Surface Chemistry in an Oil-in-Water Dispersion and Comparison of Behaviors of Individual and Clustered Iron Oxide Nanoparticles, Journal of the American Chemical Society, 17724-17732, 132 (2010) .

[13] E.S. Guang Choo, X. Tang, Y. Sheng, B. Shuter, J. Xue, Controlled loading of superparamagnetic nanoparticles in fluorescent nanogels as effective T2-weighted MRI contrast agents, Journal of Materials Chemistry, 2310-2319, 21 (2011).

[14] X.A. Xie, C.F. Zhang, Controllable Assembly of Hydrophobic Superparamagnetic Iron Oxide Nanoparticle with mPEG-PLA Copolymer and Its Effect on MR Transverse Relaxation Rate, Journal of Nanomaterials, 152524, (2011).

[15] N. Nasongkla, E. Bey, J. Ren, H. Ai, C. Khemtong, J.S. Guthi, S.-F. Chin, A.D. Sherry, D.A. Boothman, J. Gao, Multifunctional Polymeric Micelles as Cancer-Targeted, MRI-Ultrasensitive Drug Delivery Systems, Nano Letters, 2427-2430, 6 (2006).

[16] L.L. Ma, M.D. Feldman, J.M. Tam, A.S. Paranjape, K.K. Cheruku, T.A. Larson, J.O. Tam, D.R. Ingram, V. Paramita, J.W. Villard, J.T. Jenkins, T. Wang, G.D. Clarke, R. Asmis, K. Sokolov, B. Chandrasekar, T.E. Milner, K.P. Johnston, Small Multifunctional Nanoclusters (Nanoroses) for Targeted Cellular Imaging and Therapy, ACS Nano, 2686-2696, 3 (2009) .

[17] M. Liong, H. Shao, J.B. Haun, H. Lee, R. Weissleder, Carboxymethylated Polyvinyl Alcohol Stabilizes Doped Ferrofluids for Biological Applications, Advanced Materials, 5168-5172, 22 (2010).

[18] J. Lee, J. Yang, H. Ko, S. Oh, J. Kang, J. Son, K. Lee, S.W. Lee, H.G. Yoon, J.S. Suh, Y.M. Huh, S. Haam, Multifunctional Magnetic Gold Nanocomposites: Human Epithelial Cancer Detection via Magnetic Resonance Imaging and Localized Synchronous Therapy, Advanced Functional Materials, 258-264, 18 (2008).

[19] S. Sun, H. Zeng, D.B. Robinson, S. Raoux, P.M. Rice, S.X. Wang, G. Li, Monodisperse MFe2O4 (M = Fe, Co, Mn) Nanoparticles, Journal of the American Chemical Society, 273-279, 126 (2003).

[20] Q. Zhang, J.-B. Joo, Z. Lu, M. Dahl, D. Oliveira, M. Ye, Y. Yin, Self-assembly and photocatalysis of mesoporous TiO₂ nanocrystal clusters, Nano Research, 103-114, 4 (2011).

[21] E.E. Finney, R.G. Finke, Nanocluster nucleation and growth kinetic and mechanistic studies: A review emphasizing transition-metal nanoclusters, Journal of Colloid and Interface Science, 351-374, 317 (2008).